J. Fluid Mech. (1997), *vol.* 349, *pp.* 67–94. Printed in the United Kingdom

Thickness and volume measurements of a Richtmyer–Meshkov instability-induced mixing zone in a square shock tube

By G. JOURDAN[1], L. HOUAS[1], J.-F. HAAS[2] AND G. BEN-DOR[3]

[1]IUSTI, UMR CNRS 6595, Université de Provence, Technopôle de Château Gombert, 5 rue Enrico Fermi, 13453 Marseille Cedex 13, France

[2]CEA, Vaujours-Moronvilliers, BP 7, 77181 Courtry, France

[3]Pearlstone Center for Aeronautical Engineering Studies, Department of Mechanical Engineering, Ben-Gurion, University of the Negev, Beer Sheva, Israel

(Received 24 June 1996 and in revised form 23 May 1997)

A simultaneous three-directional laser absorption technique for the study of a shock-induced Richtmyer–Meshkov instability mixing zone is reported. It is an improvement of a CO_2 laser absorption technique, using three detectors during the same run, through three different directions of the test section, for the simultaneous thickness measurement of the mixing zone near the corner, near the wall and at the centre of a square-cross-section shock tube. The three-dimensional mean front and rear shapes of the mixing zone, its thickness and volume are deduced from the experimental measurements. The cases when the shock wave passes from a heavy gas to a light one, from one gas to another of similar densities and from a light gas to a heavy one, are investigated before and after the mixing zone compression by the reflected shock, for different incident shock wave Mach numbers. It is shown that the mixing zone is strongly deformed by the wall boundary layer when it becomes turbulent. Consequently, the thickness of the mixing zone is not constant along the shock tube cross-section, and the measurement of the mean volume of the mixing zone appears to be more appropriate than its mean thickness at the centre of the shock tube. The influence of the incident shock wave Mach number is also studied. When the Atwood number tends to zero, we observe a limit-like regime and the thickness, or the volume, of the mixing zone no longer varies with the incident shock wave Mach number. Furthermore, a series of experiments undertaken with an Atwood number close to zero enabled us to define a membrane-induced minimum mixing thickness, L_0, depending on the initial configuration of the experiments. From the experimental data, a hypothesis about the mixing zone thickness evolution law with time is deduced on the basis of L_0. The results are found to follow two very different laws depending on whether they are considered before or after the establishment of the plenary turbulent regime. However, no general trend can be determined to describe the entire phenomenon, i.e. from the initial conditions until the turbulent stage.

1. Introduction

The passage of a plane shock wave through an interface separating two fluids of different densities, ρ_1 and ρ_2, results in the growth of the amplitude of the

perturbations present at the interface. This process is often referred to as Richtmyer–Meshkov (Richtmyer 1960; Meshkov 1969) instability. At the final stages of the interface evolution, vortex structures, resulting from the initial misalignment of the pressure gradient of the shock wave and the density gradient across the interface, induce the creation of a turbulent mixing region which separates the pure shocked fluids. Richtmyer (1960) showed that the interface perturbation amplitude $\eta(t)$ can be described, within an error of 5–10%, by the equation

$$\frac{\mathrm{d}\eta(t)}{\mathrm{d}t} = k\,\Delta U\,A'\,\eta_0' \tag{1.1}$$

where k is the wavenumber of the perturbation ($k = 2\pi/\lambda$ where λ is the wavelength of the perturbation), ΔU is the velocity jump of the interface across the shock, A' is the post-shock Atwood number, $A' = (\rho_2 - \rho_1)/(\rho_2 + \rho_1)$, and η_0' the initial amplitude of the perturbation, and t is the time. The solution obtained by Richtmyer is valid as long as $\eta k \ll 1$. An experimental study carried out by Meshkov (1969), for relatively weak shock waves ($M < 1.6$), confirmed the linear evolution of a single-scale perturbation for both the light/heavy and the heavy/light cases.

This interface instability problem is fundamental in diverse domains, such as inertial confinement-fusion (Lindl & Mead 1975), high-enthalpy reflected shock tunnels (Stalker & Crane 1978), supersonic combustion (Waitz, Marble & Zukoski 1991), or astrophysics since Rayleigh–Taylor instability (Rayleigh 1883, Taylor 1950) occurs in supernova core collapse (Smarr *et al.* 1981).

Following the work of Andronov *et al.* (1976), many shock tube experiments have been undertaken to measure the thickness of the turbulent mixing zone induced by the instability. Owing to its impulsive and compressible nature, the shock-induced Richtmyer–Meshkov instability does not lead to a well-defined self-similar law for the mixing zone thickness. Up to now, two theories concerning the temporal thickness evolution have been used to predict the evolution of the mixing zone (Barenblatt 1983; Youngs 1984; Read 1984; Mikaelian 1985, 1990; Zaytsev *et al.* 1985; Brouillette 1989; Neuvazhayev 1991; Brouillette & Sturtevant 1993, Alon *et al.* 1995, Shvarts *et al.* 1995 and Houas & Chemouni 1996). The first is a straightforward transposition of the evolution of the Rayleigh–Taylor instability-induced mixing zone thickness, L, to the impulsive case and yields:

$$L \propto A\,\Delta U\,t. \tag{1.2}$$

The second, based on a turbulent diffusion argument, is proportional to a t^{α} power law, where $\alpha \leqslant \frac{2}{3}$. In a theoretical study, Barenblatt (1983) expressed the thickness of the mixing zone as

$$L \propto t^{\alpha} \tag{1.3}$$

where $\alpha = \frac{2}{3}$ without viscous effects and $\alpha < \frac{2}{3}$ in the presence of viscosity.

Which of these two laws better represents shock tube experiments is still an open question. To study the turbulent mixing evolution induced by Rayleigh–Taylor or Richtmyer–Meshkov instabilities, specific experiments are required to test theoretical approximations and to determine phenomenological parameters. Shock tube facilities provide flow fields relatively simply, but they also introduce many disruptive factors, which must be taken into consideration to explain the differences between theory and experiment as well as difficulties in providing a mixing zone time evolution law. The disruptive factors are: the rupture mode of the membrane used for separating the

gases; the use of a grid membrane support; the dimensions of the test section; the wall boundary layer; and the ambiguity inherent in the diagnostic method.

The first problem is due to the presence of a membrane which initially forms the interface separating the two test gases. In the present experiments, a thin mylar membrane (1.5 μm thick), produced by Dupont-de-Nemours, was used. In order to reduce the disruptive influence of the membrane, other laboratories have used home-made weaker microfilms (0.5 μm thick).

The effect of the separating membrane on the mixing depends on its density, thickness, homogeneity, mechanical and thermal properties (Houas & Chemouni 1996). As the film has a density at least 3 orders of magnitude larger than the gas density, its fragments may influence significantly the turbulent mixing growth rate (Abakumov *et al.* 1993, 1995*a*). This effect is not easy to simulate. If there is a thickness variation about its mean value, the differential acceleration of the thinner and thicker regions of the film can act as a source of initial perturbation, even in the case of a planar initial geometry. In the absence of sufficiently large thickness variations, after the incident shock acceleration, the film breaks only at the walls and then may stabilize the interface completely and suppress the mixing zone growth at least until the re-shock phase.

Erez *et al.* (1995) showed that, because of the film thermal properties, they also measured an artefact, namely the aerosol resulting from the disintegrated membrane, and apparently both the gas mixing and the presence of the aerosol contributed to the mixing width. Zaytsev *et al.* (1985) showed that the membrane could be pyrolized by strong shocks and its gaseous decomposition products behaved as a continuous interface between the two gases originally separated by the membrane.

The development of turbulent mixing models for simulating such experiments requires a knowledge of the initial conditions generating the Richtmyer–Meshkov instability (typical wavelength and amplitude) which is influenced by the membrane behaviour. A grid positioned directly downstream of the membrane can be very useful to support the membrane during the preparation of the experiment (gas filling) and to slice it into fragments of known size at the initial shock–membrane interaction. The wavelength(s) of the three-dimensional initial perturbation(s) is (are) determined by the grid geometry. The amplitude of the initial perturbation may be estimated if the mechanical properties of the membrane material are known. A possible scenario of the initial shock interaction is the following: the incident shock wave is first reflected from the membrane; then the high pressure, induced by the reflected shock wave, accelerates the membrane (thus creating a growing three-dimensional perturbation) which in turn sends compression waves into the gas downstream of it. These compression waves eventually converge to form the transmitted shock wave (Bird 1957; Meyer 1957 and Benjamin 1991). The stresses of the membrane are maximal along the wires of the grid. When the limit stresses are reached, the membrane ruptures allowing the interface to accelerate. Its bulge at the time of rupture can be considered as an initial perturbation. As this is difficult to measure at the time of the shock interaction, test rigs for dynamic loading of the membranes have been used to obtain the strain–stress relation (Abakumov *et al.* 1995*b*). It should be noted that the grid dimensions should be chosen in such a way that they do not lead to a significant level of wake turbulence.

The dimensions and the geometry of the shock tube cross-section are two important parameters. A tube of large cross-section is particularly useful in order to reduce the disruptive wall effects. Vetter & Sturtevant (1995) used a test section much larger than in previous experiments, in which a flat plate was positioned with its leading edge just upstream of the observation zone in order to better visualize the wall effects. They

showed that such an experimental facility cancelled the strong wall vortex and allowed an unambiguous interpretation of the flow visualization results. Evidently, a circular cross-section would avoid the generation corner vortices seen in the experiments with rectangular cross-sections.

Finally, the incident shock wave Mach number can also have a great influence. For high-Mach-number experiments ($M > 3$), the wall boundary layer, developing behind the transmitted shock wave, is thicker than for low Mach numbers ($M < 1.5$), even if at high Mach numbers, the film influence can be reduced because of pyrolization.

These various disruptive effects lead to a three-dimensional turbulent flow which is difficult to describe, and where classical integrated visualization techniques such as schlieren or shadowgraph (Meshkov 1969; Jacobs 1992; Brouillette & Sturtevant 1993; Rodriguez *et al.* 1993 and Houas & Chemouni 1996) provide sometimes ambiguous results for the thickness. Hence, considerable efforts have been aimed at developing more accurate methods for the measurement of the mixing zone thickness. Some of the quantitative diagnostics are of integrative type: while the absorption of X-rays (Bonazza & Sturtevant 1993) by the heavy gas, xenon, in the mixture is well suited to both turbulent and laminar diffusion zones (Galametz 1994), the Mach–Zehnder (Zaytsev *et al.* 1985) and the differential interferometries (Galametz 1994) are limited to non-turbulent mixing zones. The laser light sheet technique (Jacobs *et al.* 1993, Landeg *et al.* 1993) offers the least ambiguous method for characterizing mixing zones by excluding the signature of wall structures.

In the present work, a new diagnostic technique based on simultaneous absorption of three laser beams along three directions by one of the two constituents of the mixing zone was used. Its aim was to overcome the ambiguity inherent to any integrating technique such as the single-beam absorption method developed earlier by Fortes, Ramdani & Houas (1994). This technique yields simultaneous density profiles (i.e. only one run is necessary for data processing) in three regions within the mixing zone: in the centre (far from the wall effects), near the walls and near the corners of the shock tube. A similar, but not simultaneous, technique was previously developed by Houas, Touat & Jourdan (1995), which was able to provide more accurate thickness measurements of the mixing zone based on the interpretation of the concentration profile within the mixing zone itself. The non-uniformity of the mixing zone thickness along the entire shock tube cross-section suggested the importance of knowledge of its volume for further investigations.

2. Experiments

2.1. *Experimental set-up*

The experiments were performed in a double-diaphragm 8 m horizontal shock tube. The cross-section of the test chamber was 8.5 cm $\times$ 8.5 cm, and its length was 115 cm downstream of the second diaphragm. This enabled the investigation of the mixing zone prior to the return of the reflected shock from the endwall. The shock tube endwall was movable and permitted the control of the position of the interaction between the incident mixing zone and the first reflected shock wave. The test gases were CO_2, because of its spectroscopic properties, upstream, and helium, argon or krypton downstream. Noble gases were chosen because they did not absorb the infrared light in the range of the experiment, and because they prevented the bifurcation of the reflected shock wave. Change of the downstream gas enabled the study of the influence of the initial density configuration of the mixing zone: heavy/light for

Gas	CO_2	He	Ar	Kr
Molecular mass (kg kmol^{-1})	44	8.2	40	83.8
Density (kg m^{-3})	2.71×10^{-2}	4.19×10^{-3}	2.46×10^{-2}	5.16×10^{-2}
Specific heat capacities ratio	1.29	1.6	$\frac{5}{3}$	$\frac{5}{3}$
Viscosity (N s m^{-2})	3.56×10^{-5}	2.63×10^{-5}	4.87×10^{-5}	6.01×10^{-5}
Kinematic viscosity (m^2 s^{-1})	1.31×10^{-3}	6.28×10^{-3}	1.98×10^{-3}	1.16×10^{-3}
Diffusion coefficient in CO_2 (cm^2 s^{-1})	27.3	125.3	34	26.53

TABLE 1. Test gas properties at 25°C and 1500 Pa (with 15% air-polluted He)

CO_2/He, approximately equal densities for CO_2/Ar and light/heavy for CO_2/Kr. The gases were initially separated by a 1.5 μm plastic membrane (mylar), held over a square grid. Note that the manufacturer gave a membrane thickness variation of about zero. Some relevant properties of CO_2, He, Ar and Kr, at the initial conditions, 25°C and 1500 Pa are given in table 1. As will be shown subsequently, the helium was polluted by air during the gas filling. The effect of this pollution is noticable in the properties listed in table 1.

Figure 1 presents schematically the general experimental set-up.

The continuous wave CO_2 laser (SAT C7, 8 W power, 2 mm beam diameter and 3.1 mrad divergence) was stabilized on a suitable chosen line, and Ge and ZnSe attenuators were used so that the incident laser beam power was less than 10 mW. The simultaneous probing of three different regions of the shock tube cross-section was achieved by the simultaneous use of three infrared detectors, ZnSe mirrors and beam splitters positioned along the optical path of the incident laser beam. The three infrared detectors CdHgTe (Belov Technology), centred on 10.6 μm, were cooled with liquid nitrogen and measured the absorption of the continuous CO_2 laser beam as the mixing zone passed by. The infrared detector voltages were recorded and stored on a digitizing oscilloscope (Tektronix bandwidth 150 MHz). The signals were then transferred to a PC computer to be processed later.

2.2. *Diagnostic method*

The laser absorption principle of measurement has been described by Fortes *et al.* (1994). The absorption coefficient, at a determined frequency, α_v, depends on the temperature T and the density ρ of the absorbing medium (CO_2 in the present study), i.e.

$$\alpha_v = f(T, \rho). \tag{2.1}$$

If thermodynamic equilibrium is assumed then by a simultaneous measurement with two different wavelengths, v_1 and v_2, the problem reduces to the solution of the following two equations:

$$\alpha_{v_1} = f(T, \rho_{CO_2}), \quad \alpha_{v_2} = f(T, \rho_{CO_2}), \tag{2.2}$$

where the unknowns T and ρ_{CO_2} are the mean temperature and density profiles of the absorbing medium (CO_2 in the present case). Note that α_{v_1} and α_{v_2} which are measured, are known.

The aim of the work was to apply this spectroscopic method for thickness and volume determinations, by considering the part 10%—90% of the resulting concentration profiles of CO_2.

Inspired by the idea of Wang (1976), suggesting the additivity of the optical

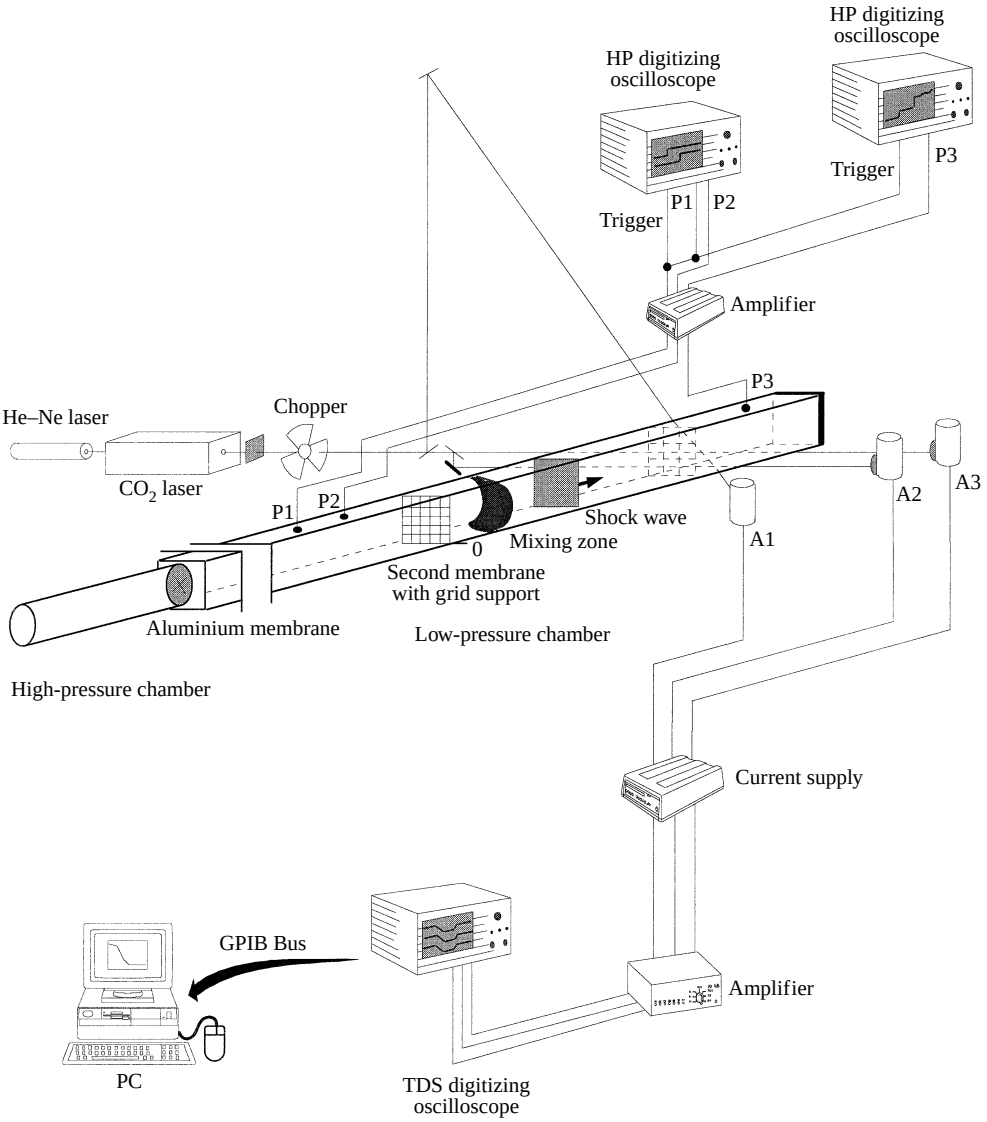

P: PCB pressure transducters —— ZnSe beam-splitters 50%–50%

A: Belov Technology infrared detectors —— ZnSe plan mirrors

FIGURE 1. Schematic illustration of the experimental set-up.

paths, and assuming the mixing zone to be multidimensional, i.e. non-uniform across the test section, the test chamber cross-section was conceptually divided into nine identical square sub-regions where, in each one, the mixing zone was considered to be one-dimensional (Houas *et al.* 1995). As shown by preliminary results (Jourdan *et al.* 1994) the mixing zone was found to be invariant to a rotation of 90° about the shock tube axis. Consequently, only three simultaneous laser beams traversing the test section near one corner, near one wall and across the centre of the shock tube

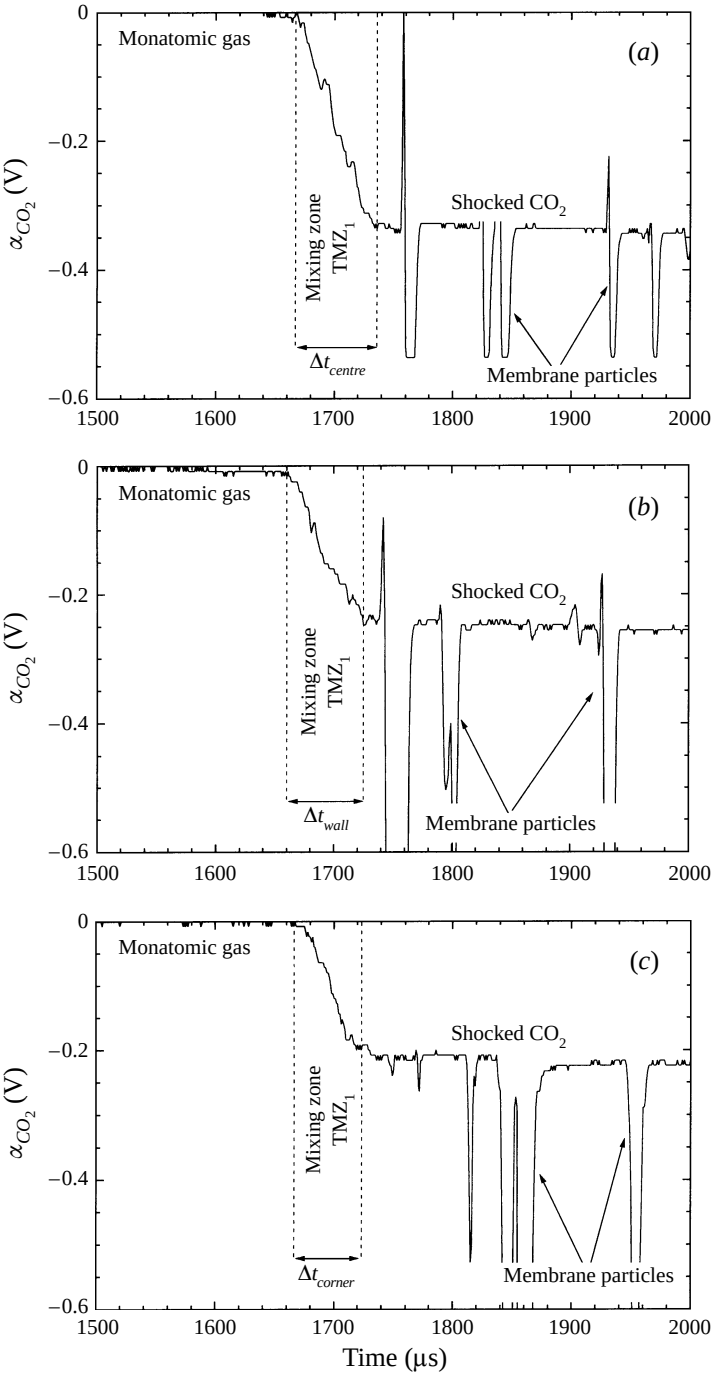

FIGURE 2. Example of typical experimental simultaneous absorption signals in the centre (*a*), near the walls (*b*) and near the corner (*c*) of the shock tube square cross-section, obtained at 55 cm from the initial position of the interface for the case CO_2/Ar. The shock wave Mach number in CO_2 is 3.1.

as shown in figure 1 were needed. Figure 2 gives an example of three simultaneous typical absorption signals, recorded on three such beams, respectively traversing the centre (figure 2*a*), close and parallel to one wall (figure 2*b*) and at 45° across one corner (figure 2*c*) of the shock tube, obtained at 55 cm from the initial position of the interface for the CO_2/Ar case with an incident shock wave Mach number of about 3.1 in CO_2. The three absorption signals were deconvoluted in order to distinguish between the contributions of the centre, the wall and the corner sub-regions (Houas *et al.* 1995). Of course, the different time durations of the mixing zone passage, Δt_{centre}, Δt_{wall} and Δt_{corner}, and its velocity, which was assumed to be constant between shocks, allowed a good estimation of its thickness in the three characteristic regions of the shock tube. However, it was shown that the present method provided more accurate thickness measurements, when considering the part 10% – 90% of the resultant concentration profile within the mixing zone itself (Houas *et al.* 1995). In addition, the simultaneous use of three detectors in one run enabled us to obtain a three-dimensional visualization of the mixing zone shape. The three-dimensional shapes of the front and rear parts of the mixing zone were approximated by the following paraboloidal functions:

$$f_{front}(x, y) = a_f x^2 + b_f y^2 + c_f, \quad f_{rear}(x, y) = a_r x^2 + b_r y^2 + c_r, \tag{2.3}$$

where the constants a_i, b_i and c_i $(i = r, f)$ were determined by the experimental measurements in the centre, near the wall and near the corner of the shock tube. Then an experimental volume of the mixing zone was defined:

$$V_{total} = \int\int f_{front}(x, y)\mathrm{d}x\,\mathrm{d}y - \int\int f_{rear}(x, y)\mathrm{d}x\,\mathrm{d}y \tag{2.4}$$

A simple approximation of the volume of the mixing zone was calculated from

$$V_{total} = \left(\tfrac{1}{3}a\right)^2 [L_{centre} + 4\,L_{wall} + 4\,L_{corner}] \tag{2.5}$$

where a is the width of the square-cross-section and L_i (i = centre, wall, corner) are the thicknesses measured in the three different regions of the test section. It was shown that (2.5) is a good approximation of (2.4) in the case of weak deformations of the mixing zone. For the study of the time evolution of the mixing zone, the mean volume of the three-dimensional mixing zone, as defined here, was found to be a better single parameter to consider than the individual thickness. The mean volume included the deformation of the mixing zone induced by the wall boundary layer effects, which are known to induce ambiguous results on the thickness measurements. Using (2.5) the approximate mean volume of the mixing zone V was calculated. Dividing it by the area of the cross-section, L_{vol} which is the thickness of a one-dimensional mixing zone of the same volume was obtained:

$$L_{vol} = \frac{V_{total}}{S} = \frac{1}{9}\,[L_{centre} + 4\,L_{wall} + 4\,L_{corner}]\,. \tag{2.6}$$

The decision to use the total mixed volume (i.e. L_{vol}) as the measure of the Richtmyer–Meshkov growth, in the present work, is arbitrary but it seems to be a clever choice because this parameter includes the effects of all of the artifacts presented in the introduction. Indeed, we can consider that in the volume there may be beneficial cancellations (e.g. membrane effect, wall boundary layer perturbation, etc.) which yield the best overall measure of the mixing zone.

It can also be seen in figure 2 that the membrane fragments did not perturb the mixing zone too much. Though in some experiments these fragments were ahead of the mixing zone and hence prevented the processing of experimental data, it turns out that with the use of a metallic grid, ensuring a regular rupture of the membrane, the resulting fragments were visible only in the CO_2. Figure 3(*a*) represents a sketch of the membrane and the grid assembly with 5×5 wires (steel guitar strings) of 0.2 mm diameter and 17 mm spacing. Figures 3(*b*) and 3(*c*) represent two absorption signals as recorded in the centre of the shock tube, for the same initial conditions (CO_2/He at Mach 3.1, 55 cm from the initial position of the interface), without and with the grid, respectively. As can be seen in figure 3(*b*), the presence of a presumably big piece of membrane ahead of the mixing zone did not permit processing of this signal, because it hid the front part of the mixing zone. However, as is evident in figure 3(*c*), the presence of the grid delayed the arrival of the membrane fragments.

2.3. *Initial conditions*

Three pairs of gases (CO_2/He, CO_2/Ar and CO_2/Kr) were tested and absorption measurements were conducted for different incident shock wave Mach numbers in CO_2 (2.4, 3.1, 4.5 and 5.3). This study is focused on the results obtained with Mach number 3.1, which is optimal to the experimental diagnostic method. For lower Mach numbers, the signal-to-noise ratio is too low, and for higher Mach numbers, the temperature increases to a level (about 2500 K) at which the CO_2 dissociates and the theoretical model of the CO_2 absorption coefficient is no longer valid.

Figure 4 presents the wave diagram of the present experiments, as calculated by the Rankine–Hugoniot relations ($x = 0$ and $t = 0$ correspond to the initial interface position and the instant of the oscilloscope triggering, respectively). The measurements were performed at four locations (16.4, 33.5, 55 and 77.5 cm), prior to the return of the reflected shock for an experimental chamber 115 cm long (see figure 4).

For the mixing zone investigations at 77.5 cm, after the compression the shock tube endwall was moved so that the interaction of the reflected shock with the incident mixing zone would occur upstream of this location. The total length of the experimental chamber was 88 cm for CO_2/He, 85 cm for CO_2/Ar and from 80 cm to 90 cm for CO_2/Kr. This last case could not be exploited since the quasi-tailored CO_2/Kr mixing zone led to an excessively long passage of the mixing zone, and since the temperature reached behind the reflected shock wave in the pure krypton was too high. Thus, only CO_2/He and CO_2/Ar results are presented for the situation after the reflected shock compression. The measured mixing zone velocities were 838, 647 and 535 m s^{-1} for CO_2/He, CO_2/Ar and CO_2/Kr respectively before the interaction with the reflected shock, and 298 and 52 m s^{-1} for CO_2/He and CO_2/Ar after the reflected shock compression.

Before running the experiment, both parts of the experimental chamber were pumped to a pressure of about 5 Pa and then filled with the two test gases to the same initial pressure of about 1500 Pa. The gases were considered to be pure except for helium which was estimated to be mixed with air (the air volume fraction was about 15%).The incident shock wave was generated by a pressure difference of about 3×10^5 Pa between the driver gas, N_2, and the first test gas, CO_2. Experimental points obtained from pressure gauges ($-72.7, -21.5, +36$ cm) and infrared detectors ($+16.4$, $+33.5$, $+55$ and $+77.5$ cm) which are plotted on figure 4 validate the Rankine–Hugoniot calculations. The incident shock wave in the CO_2 at rest [state 0(1)] and the transmitted shock in the monatomic gas at state [1(1)] are moving with the velocities

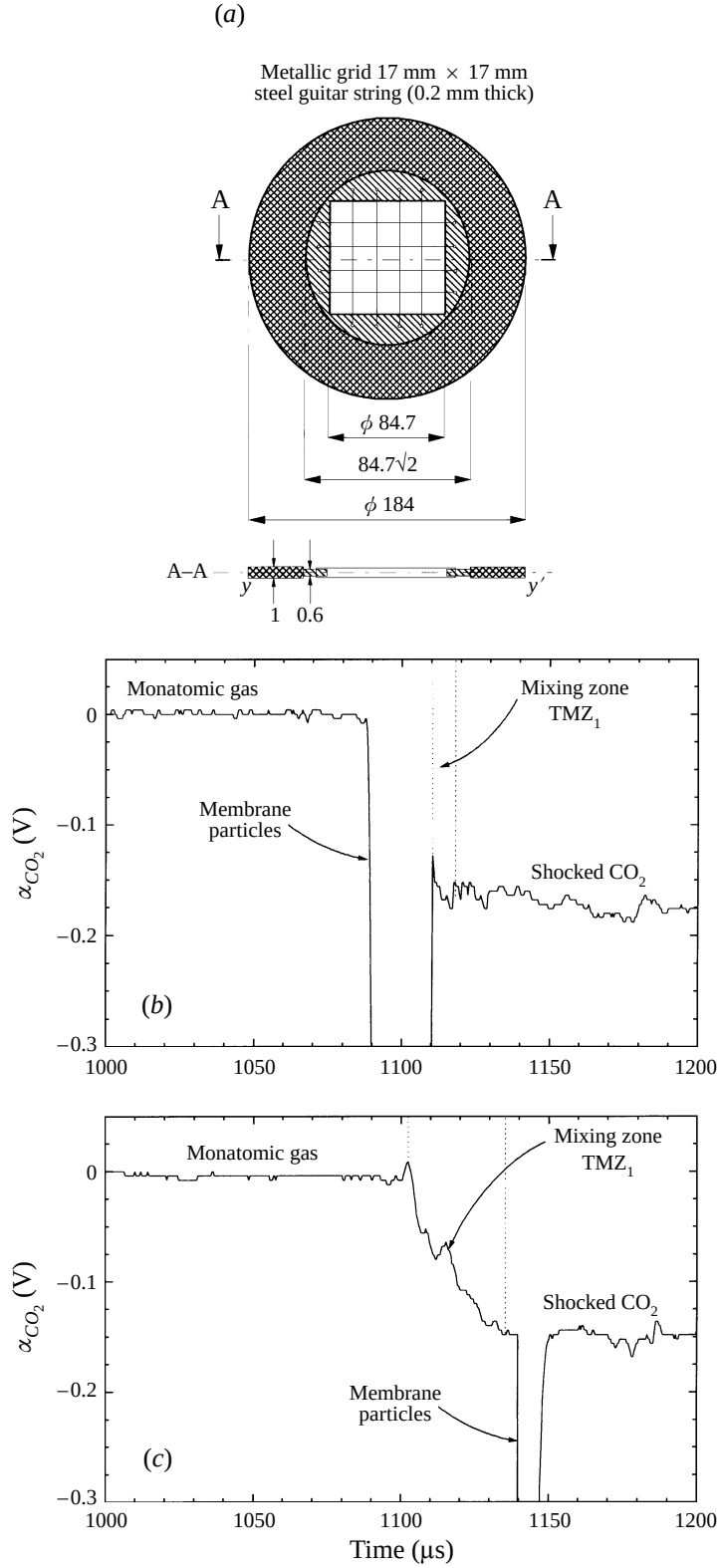

FIGURE 3. Schematic drawing of the grid membrane support (*a*) and example of absorption signals obtained for the same initial conditions as in figure 2 in the centre of the shock tube without (*b*) and with the grid (*c*).

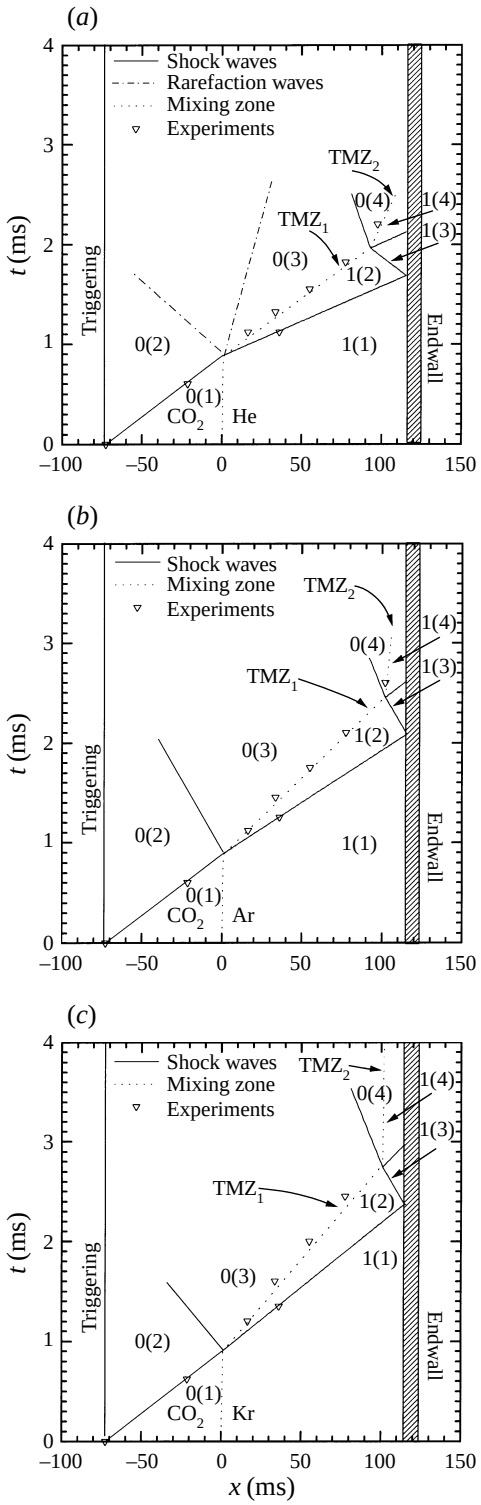

FIGURE 4. Experimental wave diagrams for (*a*) CO_2/He (heavy/light), (*b*) CO_2/Ar (similar densities) and (*c*) CO_2/Kr (light/heavy). The shock wave Mach number in CO_2 is 3.1.

	CO_2/He	CO_2/Ar	CO_2/Kr
$M_{s_{0(1)}}$	3.1	3.1	3.1
$M_{s_{1(1)}}$	2.1	3.0	3.55
$T_{1(2)}$ (K)	610	1080	1390
$P_{1(2)}$ (Pa)	6370	16610	22920
$\rho_{1(2)}$ (kg m^{-3})	1.026×10^{-2}	7.402×10^{-2}	0.1663
$U_{1(2)}$ (m s^{-1})	850	640	535
$\mu_{1(2)}$ (N s m^{-2})	3.37×10^{-5}	7.0×10^{-5}	9.03×10^{-5}
$\nu_{1(2)}$ (m^2 s^{-1})	3.28×10^{-3}	9.46×10^{-4}	5.43×10^{-4}
$T_{0(3)}$ (K)	520	630	665
$P_{0(3)}$ (Pa)	6370	16610	22920
$\rho_{0(3)}$ (kg m^{-3})	6.47×10^{-2}	0.1396	0.1828
$U_{0(3)}$ (m s^{-1})	850	640	535
$\mu_{0(3)}$ (N s m^{-2})	4.05×10^{-5}	4.25×10^{-5}	4.32×10^{-5}
$\nu_{0(3)}$ (m^2 s^{-1})	6.26×10^{-4}	3.04×10^{-4}	2.36×10^{-4}
$U_{0(4)}$ (m s^{-1})	290	55	7
A_1	−0.73	−0.31	−0.05
$A_1\Delta U_1$ (m s^{-1})	−595	−187	−26
A_2	+0.79	+0.5	+0.22
$A_2\Delta U_2$ (m s^{-1})	−442	−292	−116

TABLE 2. Flow parameters calculated from the Rankine–Hugoniot relations (with CO_2 as a pure gas and 15% air-polluted He)

$U_{s_{0(1)}}$ and $U_{s_{1(1)}}$, respectively. We can identify various features on a typical absorption signal (figure 2). At first, the maximum signal (no absorption) corresponds to the monatomic gas at rest [state 1(1)] and after the transmitted shock [state 1(2)]. Then, the decrease of the absorption signal corresponds to the passage of the incident turbulent mixing zone, denoted TMZ_1, between states 1(2) and 0(3). After the return of the shock reflected from the shock tube endwall, the compressed mixing zone TMZ_2, between states 1(4) and 0(4), is decelerated (CO_2/He and CO_2/Ar), or quasi-stopped (CO_2/Kr). To follow the evolution of the mixing zone at each location, prior to and following the compression, different runs were necessary, because all the diagnostic set-up had to be moved.

The use of helium, argon and krypton enabled us to study the influence of the Atwood number A defined by

$$A = \frac{\rho_2 - \rho_1}{\rho_2 + \rho_1} \tag{2.7}$$

where ρ_i ($i = 1, 2$) is the density of the gases (He, Ar, Kr or CO_2) taken just after the shock wave passage from gas 1 to gas 2. The Atwood numbers A_1, after the passage of the incident shock wave, were −0.73, −0.31 and −0.05 for the CO_2/He, CO_2/Ar and CO_2/Kr mixing zones, respectively. The Atwood numbers after the compression by the reflected shock wave A_2 were 0.79, 0.5 and 0.22 for CO_2/He, CO_2/Ar and CO_2/Kr, respectively. Table 2 gives all the flow parameters calculated by the Rankine–Hugoniot equations for the CO_2/He, CO_2/Ar and CO_2/Kr gas combinations, and where we consider the CO_2 as a perfect gas and also account for the pollution of helium by air.

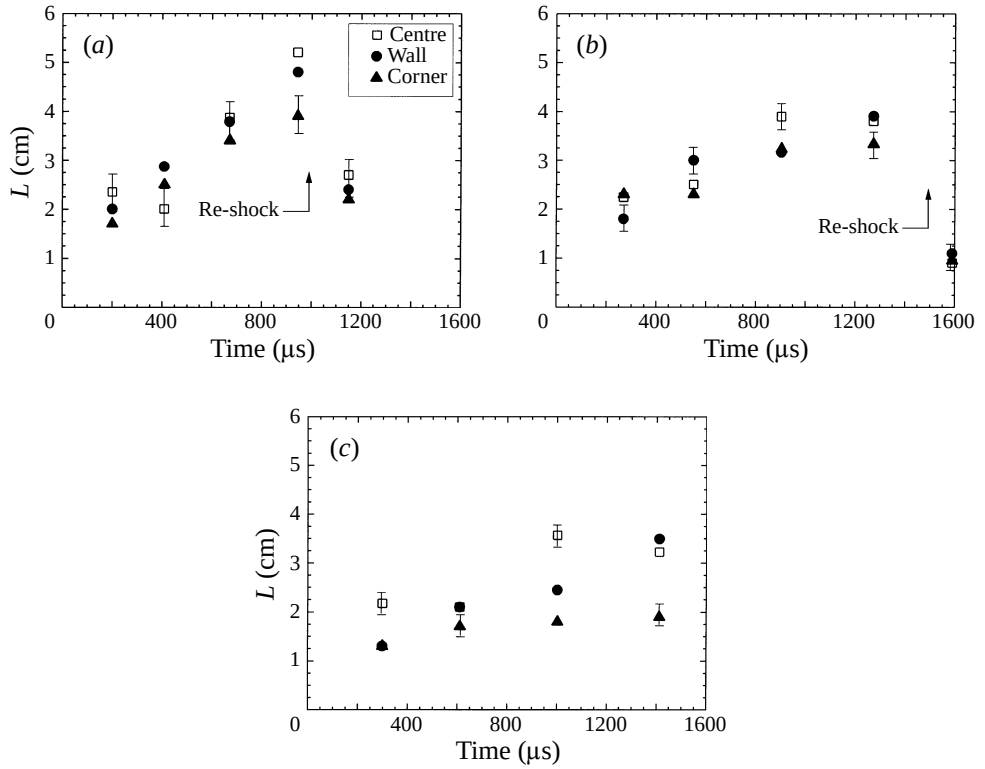

FIGURE 5. The evolution of the thickness with time, measured in the centre, near the walls and near the corners of the shock tube cross-section for (*a*) CO_2/He, (*b*) CO_2/Ar and (*c*) CO_2/Kr cases. The shock wave Mach number in CO_2 is 3.1.

3. Results and discussion

3.1. *Deformation of the mixing zone*

The error bars on the mixing zone thickness measurements are mainly due to the inaccuracy of the measurement of the time duration of the mixing zone passage on an absorption signal (such as in figure 2). They range from about ± 2 mm for the lower mixing zone velocities to ± 4 mm for the higher velocity cases. Figure 5 shows the thickness evolutions with time measured in the centre, near the walls and near the corners for each pair of gases. As expected, the CO_2/He mixing zone is thicker than that of CO_2/Ar, which is thicker than that of CO_2/Kr. These results confirm that the mixing zone thickness increases with the product $|A\,\Delta U|$ (note that $|A\,\Delta U|_{exp}^{CO_2/He} = 620$ m s^{-1}, $|A\,\Delta U|_{exp}^{CO_2/Ar} = 200$ m s^{-1} and $|A\,\Delta U|_{exp}^{CO_2/Kr} = 26$ m s^{-1}). Furthermore, for each case, the thickness measured in the centre was larger than or close to the thickness measured near the wall, and the thickness near the corner was the lowest. This implies that the mixing zone thickness was not uniform across the shock tube cross-section (Jourdan, Billiotte & Houas 1996). Consequently, thickness measurements based on integrated visualization techniques can provide ambiguous results. As can be seen in figure 5, the thickness measured in the centre of the shock tube does not follow a regular evolution; this may be due to either a large-wavelength perturbation induced by the fact that the initial membrane and the incident shock wave were not parallel, or the effect of the wall boundary layer (which stretched

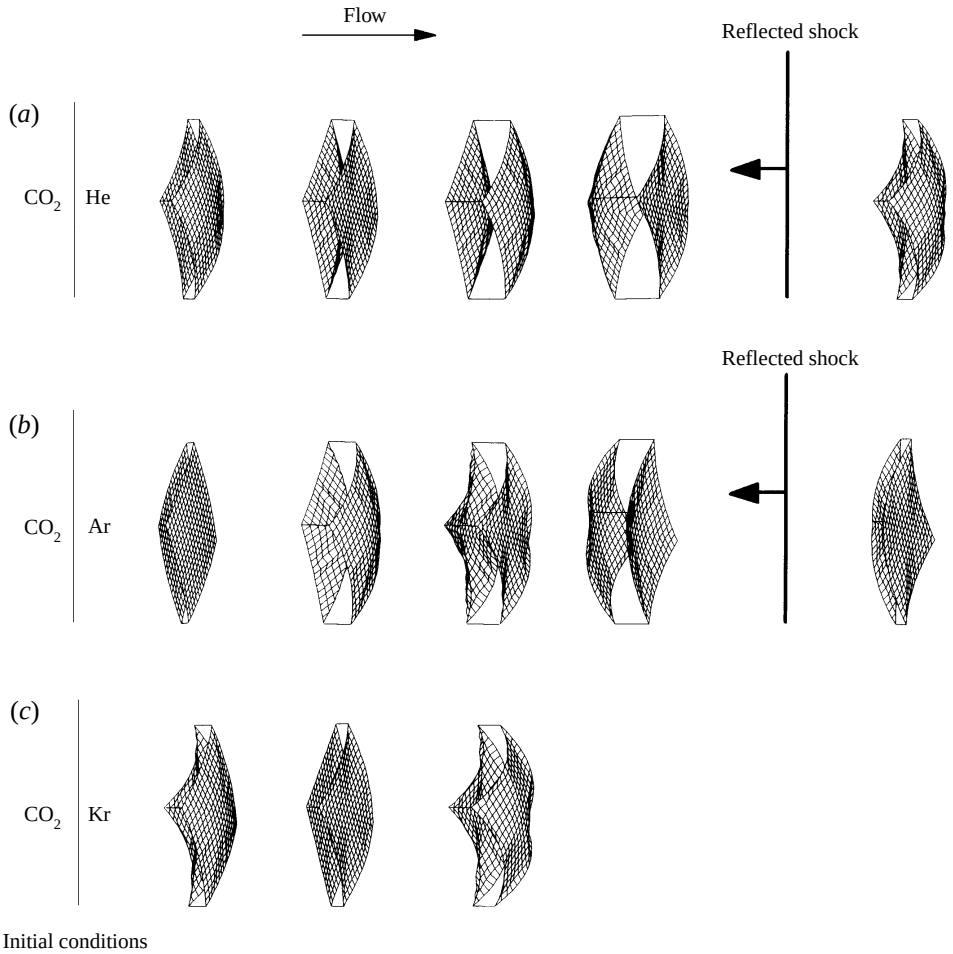

FIGURE 6. Three-dimensional representations of the mixing zone shapes at different locations for (*a*) CO_2/He, (*b*) CO_2/Ar and (*c*) CO_2/Kr mixing zones. The shock wave Mach number in CO_2 is 3.1.

the mixing to the shock tube walls), or the absence of reproducibility for the initial interface. Our analysis will be limited subsequently to the time evolution of the volume (from L_{vol}) of the mixing zone.

The effects of the compression by the reflected shock on the thickness are also presented in figure 5 for the CO_2/He and the CO_2/Ar mixing zones. The thicknesses measured 60 and 100 μs after the passage of the reflected shock for the CO_2/He (figure 5*a*) and the CO_2/Ar (figure 5*b*) cases, respectively, show that the compression factor is larger for the CO_2/Ar mixing zone (about 4) than for CO_2/He (about 2). The CO_2/Ar case is near tailored conditions and hence the stronger reflected shock compresses the gases more than the weaker first reflected shock in the CO_2/He case.

3.2. *Influence of the wall boundary layer on the mixing zone thickness measurements*

The three-dimensional approximate front and rear shapes of the mixing zone for an incident shock wave Mach number of about 3.1 in CO_2 are plotted in figure 6, for the CO_2/He, CO_2/Ar and CO_2/Kr cases, prior to and following the compression by the reflected shock. This paraboloidal representation gives only the envelope of the

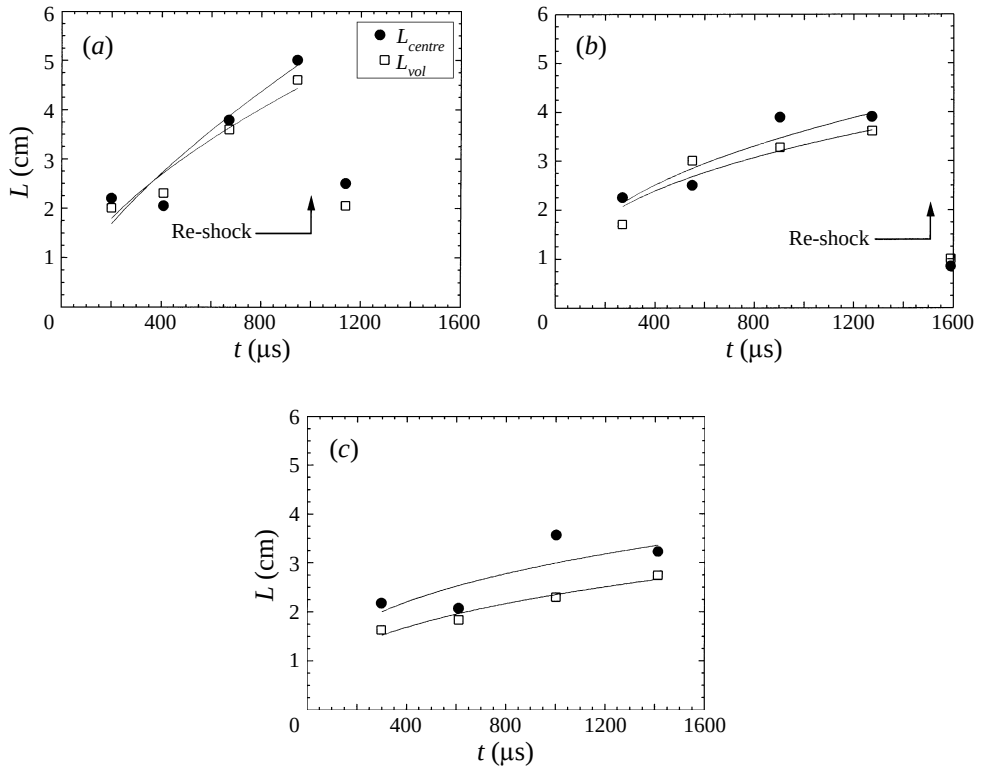

FIGURE 7. Comparison of the evolution of the mixing zone thickness measured in the centre L_{centre} with L_{vol}, for (*a*) CO_2/He, (*b*) CO_2/Ar and (*c*) CO_2/Kr pairs with time t. The shock wave Mach number in CO_2 is 3.1.

mixing zone, i.e. its mean general shape, positively or negatively bulged. The effect of the boundary layers, which stretch the mixing zone along the corners and the walls, is clearly visible. The measurements obtained after the interaction with the reflected shock show the effect of the compression on the incident turbulent mixing zone (TMZ_1). The limit of our diagnostic method is reached for the CO_2/Kr case where the high temperature (about 2600 K) in the pure krypton, following the passage of the reflected shock wave, induces a partial dissociation of the CO_2 molecules. This absorption is not accounted for in the present model. Furthermore, the development of a thick boundary layer, as discussed subsequently, limits time and location for the investigations of the CO_2/Kr mixing zone.

The CO_2/He mixing zone presents a small negative (upstream facing) bulge in the centre at the fourth location of measurement. This phenomenon appears earlier for the CO_2/Ar (third and fourth locations) and CO_2/Kr (second location but not the third). Thus, a yet unexplained reversal of the bulges for CO_2/He and CO_2/Ar is evident in figure 6.

The CO_2/He and CO_2/Ar mixing zones remain bulged in the same direction after the interaction with the reflected shock wave. This is expected since the Richtmyer–Meshkov instability predicts an amplification of the perturbation for a positive reshock Atwood number. A comparison of the mixing zone thickness in the centre L_{centre} (see figure 5) with $L_{vol} = V/S$ as calculated from equation (2.6) is presented in figure 7. If these quantities are similar, one can conclude that the mixing zone has nearly the

shape of a parallelepiped and the phenomenon under study is not much perturbed by the wall effects. However, the opposite indicates that the thickness measurements strongly depend on these disruptive effects. As can be seen, the CO_2/He mixing zone is the least perturbed by the wall boundary layers, since the difference $\Delta(L_{centre} - L_{vol})$ is small (figure 7*a*), a result which is confirmed by the three-dimensional representations (see figure 6). Unfortunatly, at 400 μs, the centreline and the volume measurements show virtually the same trend and scatter. This proves, in this case, that accounting for the total mixed volume cannot remove the glitch in the thickness shown by the centreline measurement. However, based on our few data only, we can consider this singular point as wrong.

Figures 7(*b*) and 7(*c*) show that the difference between L_{centre} and L_{vol} increases with the density of the second constituent of the mixing: argon and krypton. Moreover, when considering L_{vol}, whose evolution is more regular than L_{centre}, we cancel all the disruptive effects which sometimes provide ambiguous results.

These observations have to be correlated with the state of the wall boundary layer behind the transmitted shock wave in the monatomic gas. As the boundary layer develops behind the moving transmitted shock wave after its interaction with the contact surface, the problem of predicting transition from a laminar to a turbulent boundary layer is more complex than in classical steady flows. The studies of Hartunian, Russo & Marrone (1960) and Mirels (1964, 1984) were used to predict the state of the wall boundary layer at each location of measurement. The Reynolds number was defined by

$$Re_x = \frac{U_{s_{1(1)}} - U_{1(2)}}{\nu_{1(2)}} x \tag{3.1}$$

where $U_{s_{1(1)}}$ is the transmitted shock wave velocity, $U_{1(2)}$ is the shock-induced flow velocity, $\nu_{1(2)}$ is the kinematic viscosity of the gas in state 1(2) and x is the distance behind the shock wave. Re_x was compared with a range of values of the transition Reynolds number from about 5×10^5 to 10^6. The location where the wall boundary layer became turbulent was approximated. It was found that the CO_2/He mixing zone propagated with a laminar boundary layer until the return of the reflected shock wave. The boundary layers for the CO_2/Ar and CO_2/Kr mixing zones were already turbulent at the measurement locations 55 and 77.5 cm.

The boundary layer thickness δ was estimated using the following assumptions. We first examine the laminar case. The problem of interest is defined in figure 8(*a*), where the transmitted shock wave is moving at a constant velocity $U_{s_{1(1)}}$ into a fluid at rest and at a state described by the subscript 1(1). The state of the gas behind the shock wave, but outside the boundary layer, is denoted by the subscript 1(2). To simplify the problem, we assume that the parameters in the external flow, that is behind the shock wave, are independent of both location and time. It turns out that a problem so formulated leads to a set of similar profiles and is reduced to one single variable (Schlichting 1979):

$$\eta = \int_0^y \frac{\rho/\rho_{1(1)}}{[\nu_{1(1)}(t - x/U_{s_{1(1)}})]^{1/2}} \mathrm{d}y \tag{3.2}$$

which replaces the original three variables of space x, y and time t. Assuming that the stream function is of the form

$$\psi(x, y, t) = f(\eta) U_{1(2)} \left[\nu_{1(1)} \left(t - \frac{x}{U_{s_{1(1)}}}\right)\right]^{1/2} \tag{3.3}$$

we can describe the velocity distribution in the boundary layer by

$$u = U_{1(2)} f'(\eta) \tag{3.4}$$

By substituting these variables (u, η) into the Navier–Stokes equation, the following ordinary differential equation is obtained:

$$f'''(\eta) + \frac{1}{2}\left[\eta - \frac{U_{1(2)}}{U_{s_{1(1)}}} f(\eta)\right] f''(\eta) = 0. \tag{3.5}$$

The requisite boundary conditions are:

$$\left.\begin{array}{l} \eta = 0\colon f(\eta) = f''(\eta) = 0, \\ \eta = \infty\colon f'(\eta) = 1. \end{array}\right\} \tag{3.6}$$

The solutions of equation (3.5) are plotted in figure 8(*b*) where the constant B corresponds to the ratio $U_{1(2)}/U_{s_{1(1)}}$. The particular case $B = 0$ corresponds to the so-called Rayleigh problem. $B = 0.591$, 0.667 and 0.689 correspond to the CO_2/He, CO_2/Ar and CO_2/Kr cases, respectively. The laminar boundary layer thickness is obtained for $f'(\eta) = 0.99$ from the relation

$$\delta_{lam} = \frac{\rho_{1(1)}\, v_{1(1)} \left[t - x/U_{s_{1(1)}}\right]}{\rho_{1(2)}}\, \eta_{0.99} \tag{3.7}$$

where ρ, v, t, x correspond to the density, the kinematic viscosity, the time and the distance behind the shock, respectively. If the boundary layer is turbulent, its thickness can be estimated using the following relation defined by Mirels (1984) which is valid for air:

$$\delta_{turb} = 1.1645\; P_{1(1)}^{-1/5}\; x^{4/5} \left[\frac{(W-1)^3}{\left(W + \frac{7}{3}\right)^4}\right]^{1/5} \tag{3.8}$$

where x is the distance behind the shock in mm, $P_{1(1)}$ is the initial pressure in Pa and W corresponds to the density ratio $\rho_{1(2)}/\rho_{1(1)}$ across the shock. Table 3 gives the calculated values of δ for each case. In the CO_2/Ar and the CO_2/Kr cases, the boundary layer occupies more than 25% of the shock tube cross-sectional area, considerably reducing the flow section and modifying its fundamental properties.

In order to check and to characterize the transition in the unsteady wall boundary layer behind the transmitted shock wave, heat flux measurements were undertaken with thin-film gauges, built in the RWTH Aachen shock wave laboratory (Jessen & Grönig 1991). They were flush mounted on the wall 64.5 cm from the initial interface position. A thin-film heat flux gauge consists of a thin metal film deposited on an electrically insulating material, the substrate. The thermal conductivity of the substrate has to be much lower than that of the film. For this reason, glass (Pyrex) or ceramic (Macor) are usually used for the substrate and platinum or nickel are used for the film. These heat flux probes were used only for the detection of the transition. Therefore an absolute calibration was not necessary. Since the gauge signals were too weak, amplifying circuits were inserted in the data acquisition system. Then, the signals were filtered to eliminate noise and undesirable frequency components. The gauge response was directly proportional to the shock tube wall temperature variation ΔT_w defined by Glass & Sislian (1994). During the investigation of the boundary layer transition with a thin-film gauge, the recorded temperature variation remained constant as long as the boundary layer was laminar. When transition to turbulence occurred, the heat flux signal suddenly rose and became somewhat wavy.

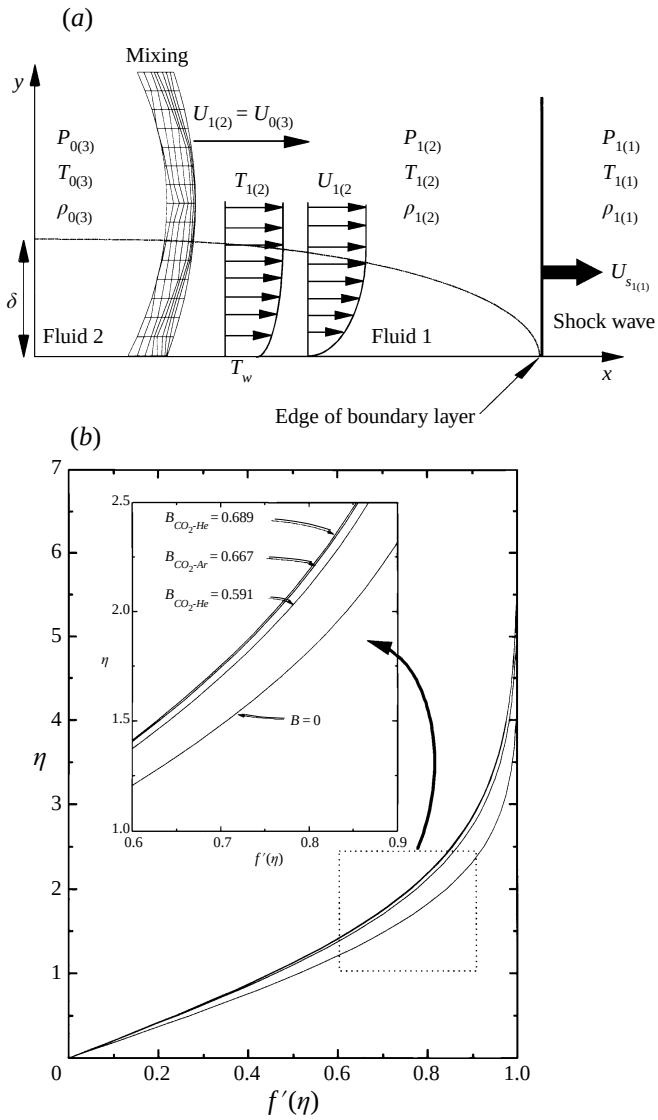

FIGURE 8. Schematic illustration of the wall boundary layer in the double-diaphragm shock tube experiments (*a*) and solutions of the differential equation describing the boundary layer conditions behind a travelling shock wave (*b*). $B = U_{1(2)}/U_{s_{1(1)}}$.

Heat flux measurements were recorded, without initial interface, in helium, argon and krypton successively, for $P_{init} = 1500$ Pa and N_2 as a driver gas, in order to isolate the transition phenomenon from the passage of the mixing zone. Figure 9 presents the experimental signals obtained when the shock wave propagated in pure helium, pure argon and pure krypton. The shock wave Mach numbers were 2.1, 3.0 and 3.6 in helium, argon and krypton, respectively. These values correspond to those of the transmitted shock wave when the incident Mach number in CO_2 was about 3.1. It is evident from figure 9(*a*) that following the incident shock wave passage (about 800 μs) ΔT_w remained constant until the return of the reflected shock wave (about 820 μs later) from the shock tube endwall. The state of the wall boundary layer was

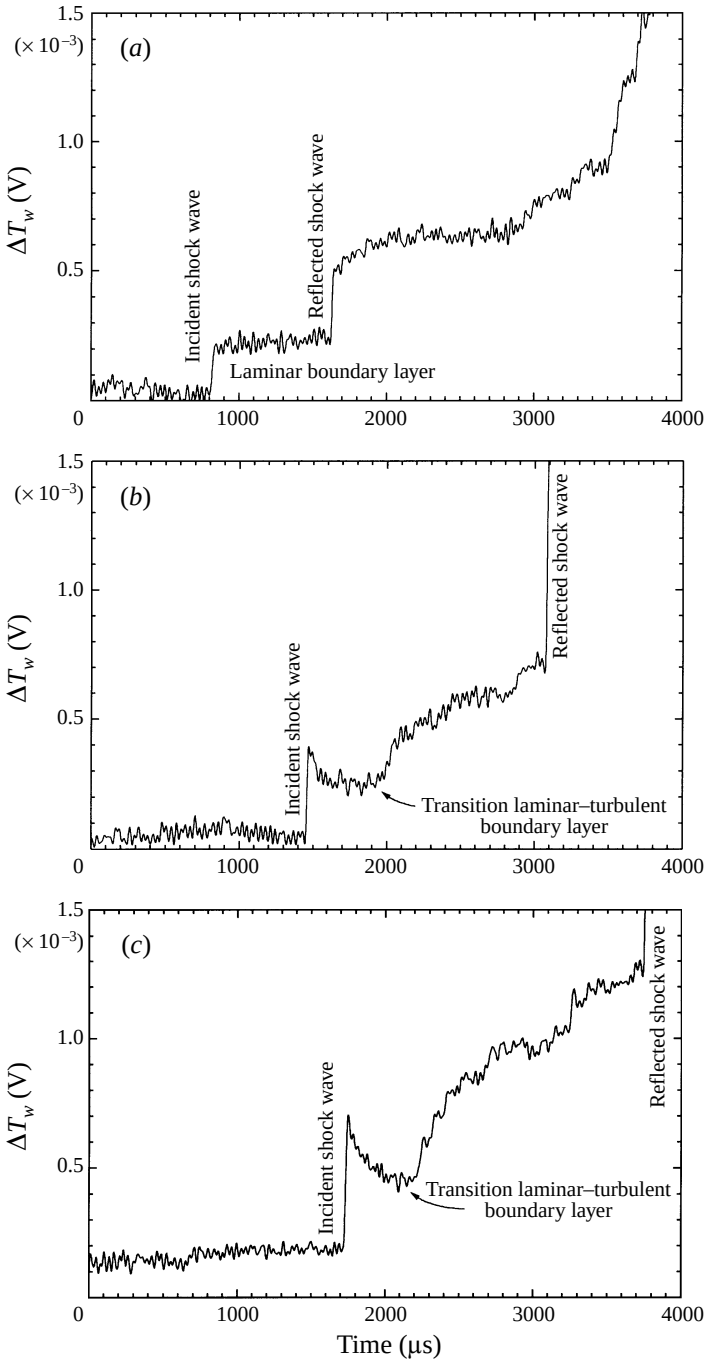

FIGURE 9. Heat flux signals obtained at 64.5 cm from the initial position of the interface in (*a*) pure helium, (*b*) pure argon and (*c*) pure krypton.

Location of the measurement (cm)	CO_2/He	CO_2/Ar	CO_2/Kr
16.4	$\delta_{lam} = 1.8$	$\delta_{lam} = 1.1$	$\delta_{lam} = 0.8$
33.5	$\delta_{lam} = 2.6$	$\delta_{lam} = 1.6$	$\delta_{lam} = 1.2$
55	$\delta_{lam} = 3.3$	$\delta_{turb} = 9.1$	$\delta_{turb} = 9.6$
77.5	$\delta_{lam} = 4.1$	$\delta_{turb} = 11.9$	$\delta_{turb} = 12.6$

TABLE 3. Laminar and turbulent boundary layer thicknesses δ (in mm), behind the transmitted shock wave, calculated from Hartunian *et al.* (1960), Mirels (1964, 1984) and Schlichting (1979)

laminar and it did not become turbulent before the reshock. The signal obtained in pure argon (figure 9*b*) presents, after the passage of the incident shock wave (at about 1450 μs), some variations and 370 μs later a continuous rise which is characteristic of a transition to a turbulent boundary layer. The reflected shock wave returned at 3100 μs and interacted with the turbulent boundary layer. According to the relative velocities of the transmitted shock wave and the incident mixing zone, the CO_2/Ar mixing zone moved with a turbulent boundary layer at a location $x > 62$ cm from the initial position of the interface. For pure krypton (see figure 9*c*), the transition (at about 2050 μs) was reached earlier, 330 μs after the passage of the incident shock wave. For a location $x > 52.5$ cm from the initial position of the interface, the CO_2/Kr mixing zone propagated with a turbulent boundary layer. As a consequence, Richtmyer–Meshkov shock tube experiments have to be treated with some caution, concerning the initial conditions, in order to reduce the wall boundary layer effects, which can considerably affect the measurements and the interpretations of the mixing zone thickness.

3.3. *Influence of the shock wave Mach number and the initial gas densities*

The evolution of the volume of the mixing zone divided by the cross-section, L_{vol}, as obtained for the different incident shock wave Mach numbers 2.4, 3.1, 4.5 and 5.3, and the three pairs of test gases are shown in figures 10(*a*) to 10(*c*), respectively. The thickness L_{vol} is seen to increase with the incident shock wave Mach number for the CO_2/He mixing zone (figure 10*a*). The growth rate (dL_{vol}/dt) of the mixing zone evolves in the same way. Figure 10(*b*) indicates that the thickness of the mixing zone for the CO_2/Ar gas combination also increases with the incident Mach number. However, unlike the CO_2/He case, here no clear conclusion can be drawn about the growth rate (dL_{vol}/dt). For the CO_2/Kr mixing zone (figure 10*c*), it is impossible to differentiate between the results for the different shock wave Mach numbers. This is quite unexpected, since the variations of the mixing zone thickness do not follow the same trend as in the previous cases. It should be noted that if these experimental results are plotted versus the location x, instead of the time, as suggested by V. Rupert (1995, personal communication), no clear pattern can be extracted. The influence of the shock wave Mach number is clear for the CO_2/He case (figure 10*a*), but the differences between the results corresponding to the lower and higher shock wave Mach numbers are smaller for the CO_2/Ar case (figure 10*b*). They vanish for CO_2/Kr (figure 10*c*). This trend is due to the fact that the corresponding Atwood numbers decrease towards 0. It should be noted that the ratios of the products $|A\,\Delta U|$ for the higher and the lower shock wave Mach numbers are about 2, 5 and 10 for the CO_2/He, CO_2/Ar and CO_2/Kr cases, respectively. Since a large ratio does not have an influence on the mixing zone behaviour when the Atwood number tends to zero,

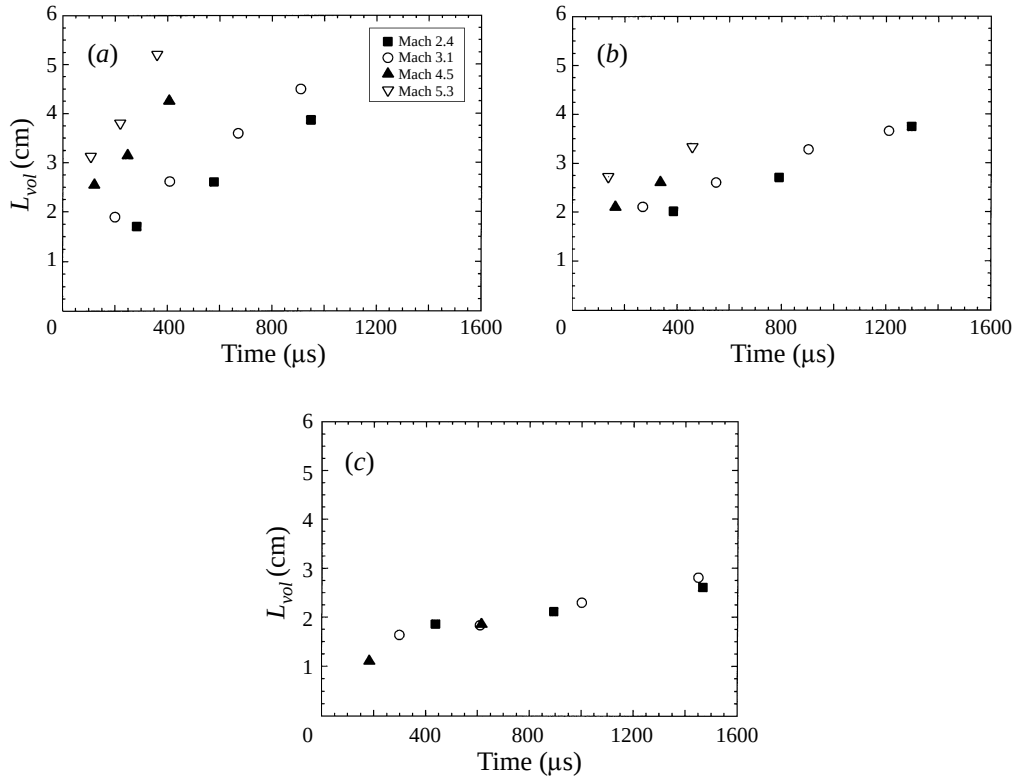

FIGURE 10. Influence of the shock wave Mach number on the evolution of the thickness L_{vol} with time t for (a) the CO_2/He, (b) the CO_2/Ar and (c) the CO_2/Kr mixing zones.

it is concluded that for the present experiments the effect of the Atwood number is more pronounced than that of the Mach number. This point is more rigorously discussed in the following subsection.

3.4. *Influence of the experimental configuration for* $A \approx 0$

Under ideal, i.e. membraneless, conditions in the absence of a post-shock density mismatch on the interface (Atwood number $A_0 = 0$) there should not be any instability or mixing between the two test gases. In order to understand the case $A \to 0$, experiments with the gas combination CO_2/CO_2, for the incident shock wave Mach numbers 2.4, 3.1 and 4.5 were conducted. The signature of a 'mixing zone' (between two regions of CO_2 which are at different thermodynamic states) with a measurable thickness was observed on the absorption profiles (figure 11a). This led us to introduce the concept of 'membrane-induced minimum mixing', which is solely induced by the influence of the experimental set-up. Without deliberate initial perturbations on the planar membrane, the mixing zone development observed in these tests suggested that there should be another source of initial perturbation induced by the membrane and its interaction with the incident shock wave. Figure 11(a) presents an example of such an absorption signal, obtained in the centre of the shock tube cross-section, at the location $x = 55$ cm, for a CO_2/CO_2 case with a shock wave Mach number of 3.1. About 100 μs after the passage of the transmitted shock wave, a decrease of the signal corresponding to the passage of a 'mixing zone' is observed, between the states $CO_{2_{1(2)}}$ and $CO_{2_{0(3)}}$. In order to understand this result, and using the previous

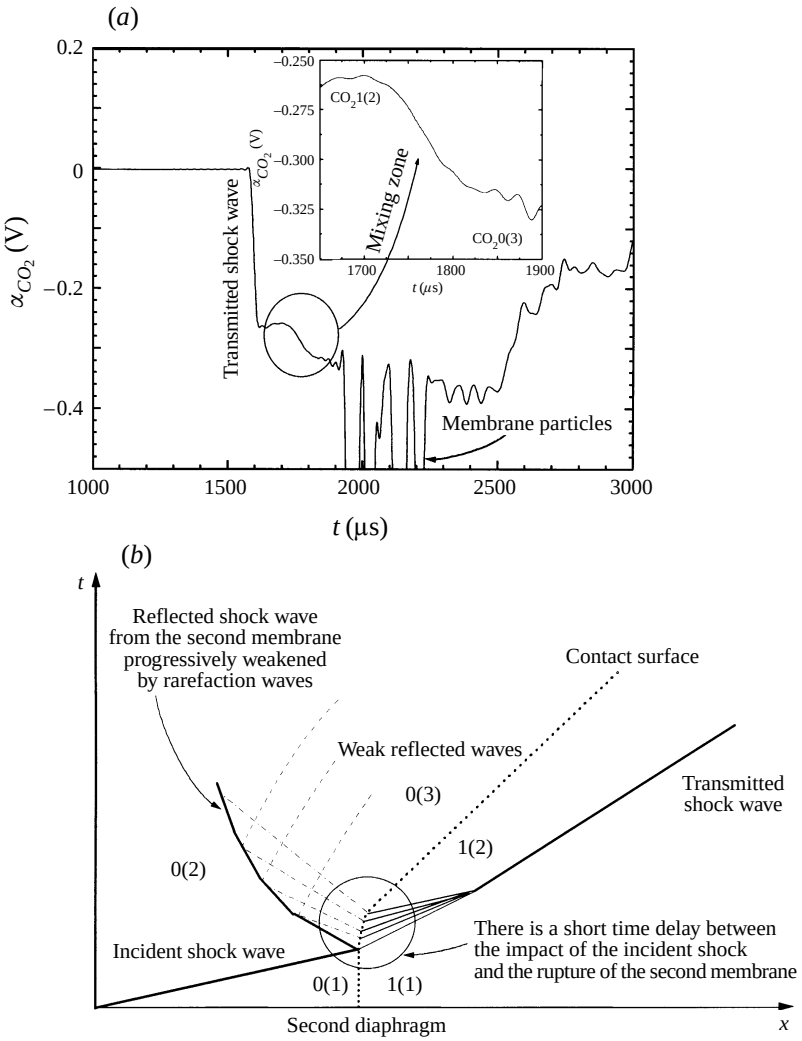

FIGURE 11. Example of an absorption signal obtained for the gas combination CO_2/CO_2 showing the presence of a mixing zone (*a*), where the incident shock wave Mach number in CO_2 is 3.1. Schematic wave diagram (*b*) of the experiment shown in (*a*) when the second membrane rupture is delayed (not to scale).

works of Bird (1957), Meyer (1957) and Benjamin (1991), the schematic wave diagram of this experiment is presented in figure 11(*b*). The real origin of this phenomenon is the nature of the interaction between the incident shock wave and the second membrane. The flow near the membrane rupture point is much more complicated when the rupture is delayed and can vary greatly with increasing time delay. The consequence is that the CO_2 on both sides of the membrane is, in fact, in different thermodynamic states after the shock wave passage. Experimentally, a decrease of the incident shock wave Mach number by about 10% was observed. This confirms the following interaction scenario. In the CO_2/CO_2 case presented, the incident shock wave Mach number of about 3.1, fell to 2.85 after transmission. The same phenomenon was observed without the grid. This illustrates the influence of the complex interaction between the incident shock wave and the membrane on the resulting flow.

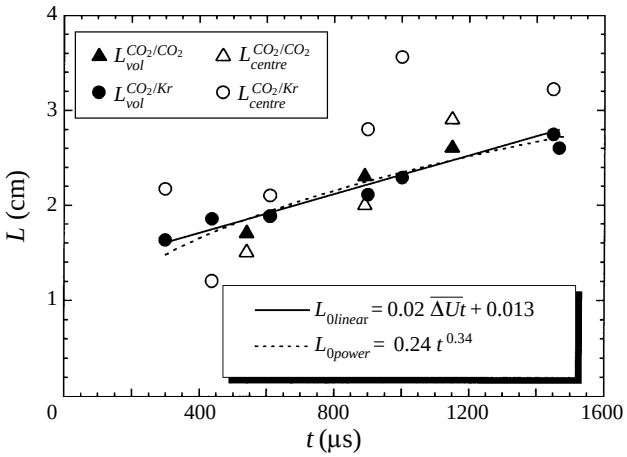

FIGURE 12. Evolution of the mixing zone thickness with time for experiments with $|A| \approx 0$. The L_{vol} experimental points are fitted with linear and power laws.

The time duration of this membrane-induced mixing zone passage is about 150 μs. Considering the three test conditions, CO_2/CO_2 for the incident shock wave Mach numbers 2.4, 3.1 and 4.5, added to the CO_2/Kr experiments with shock wave Mach numbers 2.4 and 3.1, where the post-incident-shock Atwood number was very close to zero, we have presented on figure 12 the evolution of L_{vol} and L_{centre} with time for the CO_2/Kr and CO_2/CO_2 cases, respectively. As can be seen, accounting for the mean volume of the mixing zone cancelled the scattered evolution observed at the centreline. Then, only L_{vol} experimental data have been fitted by both a linear regression and a power law. The chosen linear regression was

$$L_{0_{linear}} = a_1 t + b_1 \tag{3.9}$$

with $a_1 = 10.42$ and $b_1 = 0.013$, where $L_{0_{linear}}$ and t are in m and s, respectively. In order to compare the present work with the empirical law given by Zaytsev *et al.* (1985):

$$\frac{\mathrm{d}L}{\mathrm{d}t} = \left(a + b\,|A|\right) \Delta U \tag{3.10}$$

with $a = 0.02$ and $b = 0.07$ for the incident phase ($A < 0$), where L and ΔU are in m and m s^{-1}, respectively, we have made the following substitutions. If $A = 0$, equation (3.10) becomes

$$\frac{\mathrm{d}L}{\mathrm{d}t} = a\Delta U. \tag{3.11}$$

After integration we obtain:

$$L = a\Delta U t + \text{const.} \tag{3.12}$$

For $A = 0$, the Zaytsev *et al.* (1985) empirical relation suggests the presence of a 'minimum mixing' zone, unlike Mikaelian (1985, 1990) who proposed a theoretical thickness evolution transposed from a scaling observed for Rayleigh–Taylor experiments:

$$h_1 = 0.28\,|A\,\Delta U|\,t. \tag{3.13}$$

Let us put $L_{0_{linear}}$ in the form of equation (3.12), with $\overline{\Delta U}$ the arithmetic average of the different mixing zone velocity jumps with an Atwood number close to zero. For

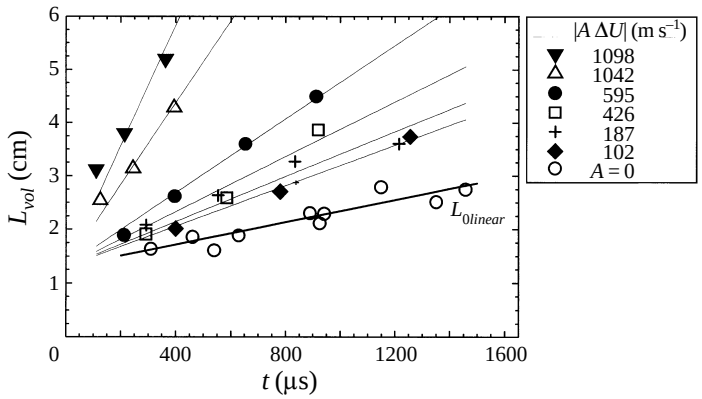

FIGURE 13. Evolution of the mixing zone thickness with time for different $|A\,\Delta U|$. The experimental points are fitted by $L = L_{0_{linear}} + k_1\,|A\,\Delta U|\,t$.

$\overline{\Delta U_{A\approx 0}} = 510$ m s^{-1}, we found (see figure 12)

$$L_{0_{linear}} = a_2\,\overline{\Delta U}\,t + b_1 \tag{3.14}$$

with $a_2 = 0.02$ and $b_1 = 0.013$. As can be seen, the value of a_2 is close to Zaytsev *et al.*'s constant *a*. The function L_0 corresponds to the 'minimum mixing zone' thickness induced by the experimental set-up when the Atwood number is close to zero. It should be noted that different functions of L_0 are appropriate to different experimental set-ups.

We have also fitted the same experimental data with a power law

$$L_{0_{power}} = c_1 t^{c_2} \tag{3.15}$$

with $c_1 = 0.24$ and $c_2 = 0.34$, where $L_{0_{power}}$ and t are in m and s, respectively. Although the fit of $L_{0_{power}}$ to the experimental points is as good as that of $L_{0_{linear}}$, at this stage c_1 and c_2 cannot be simply interpreted.

3.5. *Discussion*

In this subsection, by a synthesis of the different experimental conditions and results presented in this paper, an attempt to obtain new information on the mixing zone thickness growth law with time is made. If the influence of the product $|A\,\Delta U|$ is an accepted fact, two laws of the temporal thickness evolution can be suggested. The first law is a linear evolution with time and the second is proportional to a t^{α} power law where $\alpha \leqslant \frac{2}{3}$. The influence of the wall boundary layer in shock tube experiments and the presence of a membrane in horizontal shock tubes, or a diffusion zone created after the retraction of a separating plate before the shock wave passage in vertical shock tubes (Rodriguez *et al.* 1993; Brouillette 1989; Bonazza & Sturtevant 1993; Zaytsev, Chebotareva & Titov 1993) do not permit such a well-defined, self-similar law of the mixing zone thickening.

Considering $L_{0_{linear}}$ as a limit function of our Richtmyer–Meshkov shock tube experiments for $A = 0$, we have fitted all the other experimental data, with $A \neq 0$, by the function

$$L = L_{0_{linear}} + k_1\,|A\,\Delta U|\,t. \tag{3.16}$$

The result is shown on figure 13. The different values of the constant k_1 are presented in table 4 (with L, $|A\,\Delta U|$ and t in m, m s^{-1} and s, respectively) for each

Gas combination	$\lvert A_1\,\Delta U_1\rvert$ (m s^{-1})	A_1	k_1
CO_2/He Mach 5.3	1098	−0.72	0.094
CO_2/He Mach 4.5	1042	−0.77	0.064
CO_2/He Mach 3.1	595	−0.73	0.041
CO_2/He Mach 2.4	426	−0.74	0.036
CO_2/Ar Mach 3.1	187	−0.31	0.057
CO_2/Ar Mach 2.4	102	−0.24	0.084
CO_2/Kr Mach 3.1	26	−0.05	0
CO_2/Kr Mach 2.4	23	+0.06	0
CO_2/CO_2 Mach 4.5	62	−0.06	0
CO_2/CO_2 Mach 3.1	31	−0.05	0
CO_2/CO_2 Mach 2.4	17	−0.04	0

TABLE 4. Values of the fitting constant k_1

gas combination and $|A\,\Delta U|$ product. The thickness of the mixing zone cannot be smaller than the 'minimum mixing' described by the limit function L_0. We have also tried to fit the experimental points by power laws as t^{α} with $\alpha \leqslant \frac{2}{3}$, but the results were very poor in comparison with the linear law given in relation (3.16). In fact, the experimental points are well fitted by a power law if we consider the thickness of the mixing zone measured in the centre of the tube, and well fitted by a linear law if we consider the volume. It is our belief that the measurements of the mean volume of the mixing zone are more accurate than its mean thickness, because the second parameter is too sensitive to the part of the fluid lost towards the shock tube walls, due to the mixing zone–boundary layer deformation. In addition, the present method does not account for all the mixing lost towards the shock tube walls, hence no fundamental statement can be made about the linear or the power laws. However, the study of L_{vol} permits a better accuracy of the experimental results concerning the wall boundary layer influence. The principal effect of it is to considerably slow down the thickening of the mixing zone in the centre of the tube, favouring a power law evolution over a linear law, especially for high shock wave Mach number experiments (Houas & Chemouni 1996). On the other hand, relation (3.16) could be considered as an improvement of Zaytsev *et al.*'s empirical relation (3.10).

Finally, the time evolution of the thickness of the mixing zone measured in the centre of the shock tube could be expressed as

$$L = 0.013 + 0.02\,\overline{\Delta U_{A\approx 0}}\,t + k_1\,|A\,\Delta U|\,t - L_{\delta}. \tag{3.17}$$

In this form, the first term of relation (3.17) can be considered as the part of the mixing induced by the membrane particles and depending on the membrane material properties. The second term depends on the interaction nature of the shock wave with the membrane which initially separates the two gases, but not on the Atwood number. The third term represents the growth of the mixing zone depending on all the fundamental parameters: the Atwood number, the velocity jump of the interface and the time. The problem of the non-constant value of k_1 is that it is strongly correlated with the fourth term L_{δ}, which corresponds to the loss of mixing towards the wall of the shock tube due to the presence of the boundary layer and is in competition with the third one. For example, L_{δ} is high for both high shock wave Mach number and low pressure experimental conditions, and low for both weak shock waves and high pressures. It is clear that if the volume of the mixing zone is measured and divided by the shock tube area, then $L_{\delta} \rightarrow 0$, but we shall have $L_{\delta} \neq 0$. As the effects

of the membrane, the shock–membrane interaction, the Richtmyer–Meshkov growth and the boundary layer interaction were supposed to be linearly superposable, this strong assumption would probably produce results comparable only under conditions identical to the present experiments. However, it would be interesting to consider this type of approach in further works.

4. Conclusion

A simultaneous three-directional laser diagnostic technique was developed for thickness and volume determinations of a gaseous mixing zone originated from the Richtmyer–Meshkov instability in a square shock tube. Investigations were conducted for the cases when the shock wave passes from a heavy gas to a light one, from one gas to another of similar densities and from a light gas to a heavy one. It was found that the increase of the shock wave Mach number induced an increase of the thickness and volume of the mixing zone, but it did not seem to have a larger influence when the difference between the initial densities of the gases tended to zero. It was shown that the laminar boundary layer behind the shock wave slowly deformed the mixing zone but the deformation became pronounced when the wall boundary layer was turbulent. This result was confirmed by the three-dimensional visualizations of the mixing zone obtained from the experiments. As the thickness was not constant across the shock tube test section, the volume, instead of the thickness of the mixing zone, was chosen to be the more relevant parameter. Furthermore, it was shown that, even if the initial Atwood number was equal to zero, the initial experimental shock tube configuration, and particularly the membrane, always induced a 'mixing zone' between the two gases. This 'membrane minimum mixing thickness' resulted from the delay in the interaction of the incident shock wave and the membrane and depended essentially on the velocity jump of the interface.

Considering the time evolution of the growth of the mixing zone, and even if the present diagnostic technique enabled us to reduce the uncertainty on the part of the mixing lost towards the walls, the measurement of the mean volume, instead of the thickness of the mixing zone at the shock tube centre, has not clearly favoured the hypothesis of a linear dependence on time instead of a power law. The large cross-section shock tube which is under construction in the University of Provence, IUSTI, UMR CNRS, at Marseille will perharps enable one to better understand this point in the future.

This work is partially supported by the CEA Vaujours-Moronvilliers on contract No. 304 844/00/D1.

REFERENCES

Abakumov, A. I., Meshkov, E. E., Nizovtsev, P. N., Nikiforov, V. V. & Rogachov, V. G. 1993 Turbulent mixing zone development in shock tube experiments with thin film separation. In *Proc. 19th Intl Symp. on Shock Waves*, vol. IV, pp. 223–226. Marseille.

Abakumov, A. I., Meshkov, E. E., Nizovtsev, P. N., Nikiforov, V. V. Sadikov, N. P., Tilkunov, V. A., Tolshmyakov, A. I. Tochilin, V. O. & Kholkin, S. I. 1995*a* Shock tube experiments: Film effects on the turbulent mixing zone development. In *Proc. 5th Intl Workshop on the Physics of Compressible Turbulent Mixing*, pp. 118–123. Stony Brook (NY).

Abakumov, A. I., Gerasimov, S. I., Meshkov, E. E., Nizovtsev, P. N., Nikiforov, V. V., Tochilin, V. O. & Kholkin, S. I. 1995*b* Investigations of setup influence to turbulent mixing zone development in shock tube experiments. *Sci. Rep.* Contract CEA Vaujours-Moronvilliers/VNIIEF Sarov.

Alon, U., Hecht, J., Ofer, D. & Shvarts, D. 1995 Power laws and similarity of Rayleigh–Taylor and Richtmyer–Meshkov mixing fronts and all density ratios. *Phys. Rev. Lett.* **78**, 534–537.

Andronov, V. A., Bakhrakh, S. M., Meshkov, E. E., Mokhov, V. N., Nikiforov, V. V., Pevnitskii, A. V. & Tolshmyakov, A. I. 1976 Turbulent mixing at contact surface accelerated by shock waves. *Sov. Phys. JETP* **44**, 424–427.

Barenblatt, G. I. 1983 Self-similar turbulence propagation from an instantaneous plane source. *Non linear Dynamics and Turbulence* (ed. G. I. Barenblatt, G. Loos & D. D. Joseph). Pitman.

Benjamin, R. F. 1991 Shock and reshock of an unstable fluid interface. In *Proc. 3rd Intl Workshop on the Physics of Compressible Turbulent Mixing*, pp. 325–330. Abbey of Royaumont, France.

Bird, G. A. 1957 A note on multiple diaphragm shock tubes. British Crown Copyright, Britanic Majesty London.

Bonazza, R. & Sturtevant, B. 1993 X-ray measurements of shock-induced mixing at an *air/Xe* interface. In *Proc. 4th Intl Workshop on the Physics of Compressible Turbulent Mixing*, pp. 194–200. Cambridge.

Brouillette, M. 1989 On the interaction of shock waves with contact surfaces between gases of different densities. PhD thesis, California Institute of Technology, Pasadena.

Brouillette, M. & Sturtevant, B. 1993 Experiments on the Richtmyer–Meshkov instability: Small-scale perturbations on a plane interface. *Phys. Fluids* A **5**, 916–930.

Erez, L., Sadot, O., Erez, G. & Levin, L. A. 1995 Effect of the membrane on measurements of turbulent mixing in shock tubes. In *Proc. 5th Intl Workshop on the Physics of Compressible Turbulent Mixing*, pp. 169–177. Stony Brook (NY).

Fortes, J., Ramdani, A. & Houas, L. 1994 CO_2 laser absorption measurements of temperature and density in shock induced Richtmyer–Meshkov mixing zone. *Phys. Rev.* E **50**, 3041–3049.

Galametz, I. 1994 Visualisation et mesure de masse volumique dans un mélange gazeux en tube á choc. PhD thesis, Université des Sciences et Technologies de Lille.

Glass, I. I. & Sislian, J. P. 1994 *Nonstationary Flows and Shock Waves,* Chap. 6, §2. Clarendon.

Hartunian, R. A., Russo, A. L. & Marrone, P. V. 1960 Boundary layer transition and heat transfer in shock tubes. *J. Aero. Sci.* **27**, 587–594.

Houas, L. & Chemouni, I. 1996 Experimental investigation of Richtmyer–Meshkov instability in shock tube. *Phys. Fluids* **8**, 614–627.

Houas, L., Touat, A. & Jourdan, G. 1995 Richtmyer–Meshkov mixing zone study by a multidirectional laser absorption technique. *Phys. Rev.* E **5-B**, 5344–5351.

Jacobs, J. W. 1992 Shock-induced mixing of a light gas cylinder. *J. Fluid. Mech.* **234**, 629–648.

Jacobs, J. W., Jenkins, D. G., Klein, D. L. & Benjamin, R. F. 1993 Experimental study of instability growth patterns of a shock-accelerated thin fluid layer. In *Proc. 4th Intl Workshop on the Physics of Compressible Turbulent Mixing*, pp. 223–229. Cambridge.

Jessen, C. & Grönig, H. 1991 A new method for manufacture of thin film heat flux gauges. *Shock Waves J.* **1**, 161–164.

Jourdan, G., Billiotte, M. & Houas, L. 1996 Shock induced Richtmyer–Meshkov instability in the presence of a wall boundary layer. *Shock Waves J.* **6**, 1–8.

Jourdan, G., Touat, A., Chemouni, I. & Houas, L. 1994 Multidirectional laser absorption technique for simultaneous determination of temperature and concentration within a shocked gaseous interface. In *Proc. 7th Intl Symp. on Application of Laser Techniques to Fluids Mechanics*, vol. 1, pp. 20.3.1–20.3.5. Lisbon.

Landeg, D., Philpott, M., Smith, I. & Smith, A. 1993 The laser sheet as a quantitative diagnostic in shock tube experiments. In *Proc. 4th Intl Workshop on the Physics of Compressible Turbulent Mixing*, pp. 230–239. Cambridge.

Lindl, J. D. & Mead, W. C. 1975 Two-dimensional simulation of fluid instability in laser-fusion pellet. *Phys. Rev. Lett.* **34**, 1273–1276.

Meshkov, E. E. 1969 Instability of a shock wave accelerated interface between two gases. *Sov. Fluid Dyn.* **4**, 107–108.

Meyer, R. F. 1957 The impact of a shock wave on a movable wall. *J. Fluid. Mech.* **4**, 309–331.

Mikaelian, K. O. 1985 Richtmyer–Meshkov instabilies in stratified fluids. *Phys. Rev.* A **31**, 410–419.

Mikaelian, K. O. 1990 Turbulent energy at accelerating and shocked interfaces. *Phys. Fluids* **2**, 592–598.

Mirels, H. 1964 Shock tube test time limitation due to turbulent wall boundary layer. *AIAA J.* **2**, 84–93.

Mirels, H. 1984 Turbulent boundary layer behind constant velocity shock including wall blowing effects. *AIAA J.* **22**, 1042–1047.

Neuvazhayev, V. E. 1991 Development of turbulent mixing zone induced by the Richtmyer–Meshkov instablity. *Maths Mod.* **10**, 3–7.

Rayleigh, Lord 1883 Investigation of the character of the equilibrium of an incompressible heavy fluid of variable density. *Proc. Lond. Math. Soc.* **14**, 170–177 (Reprinted in Scientific Papers, vol. 2, pp. 200–207, Cambridge University Press, 1900).

Read, K. I. 1984 Experimental investigation of turbulent mixing by Rayleigh–Taylor instability. *Physica* D **12**, 45–48.

Richtmyer, R. D. 1960 Taylor instability in shock acceleration of compressible fluids. *Commun. Pure Appl Maths* **13**, 297–319.

Rodriguez, G., Galametz, I., Croso, H. & Haas J. F. 1993 Richtmyer–Meshkov instability in a vertical shock tube. In *Proc. 19th Intl Symp. on Shock Waves*, vol IV, pp. 275–280. Marseille.

Schlichting, H. 1979 *Boundary Layer Theory*, 7th Edn. MacGraw-Hill.

Shvarts, D., Alon, U., Ofer, D., McCrory, R. L. & Verdon, C. P. 1995 Nonlinear evolution of multimode Rayleigh–Taylor instability in two and three dimensions. *Phys. Plasma* **2**, 2465–2472.

Smarr, L., Wilson, J. R., Barton, R. T. & Bowers, R. L. 1981 Rayleigh–Taylor overturn in supernova core collapse. *Astrophys. J.* **246**, 515–525.

Stalker, R. J. & Crane, K. C. A. 1978 Driver gas contamination in a high-enthalpy reflected shock tunnel. *AIAA J.* **16**, 277–279.

Taylor, G. I. 1950 The instability of liquid surfaces when accelerated in a direction perpendicular to their planes. *Proc. R. Soc. Lond.* A **201**, 192–196.

Vetter, M. & Sturtevant, B. 1995 Experiments on the Richtmyer–Meshkov instability of an air/SF_6 interface. *Shock Waves J.* **4**, 247–252.

Waitz, I. A., Marble, F. E. & Zukoski, E. E. 1991 An investigation of a contoured wall injector for hypervelocity mixing augmentation. *AIAA J.* **91**, 2265–2271.

Wang, J. T. 1976 Laser absorption methods for simultaneous determination of temperature and species concentration through a cross section of radiating flow. *Appl. Optics* **15**, 768–773.

Youngs, D. L. 1984 Numerical simulation of turbulent mixing by Rayleigh–Taylor instability. *Physica* D **12**, 32–44.

Zaytsev, S. G., Chebotareva, E. & Titov, S. 1993 Passage of a shock wave through a continuous interface separating gases of different densities. In *Proc. 19th Intl Symp. on Shock Waves*, vol. IV, pp. 227–232. Marseille.

Zaytsev, S. G., Lazareva, E. V., Chernuka, V. V. & Belyaev, V. M. 1985 Intensification of mixing at the interface between media of different densities upon the passage of a shock wave through it. *Dolk. Akad. Nauk. SSSR* **283**, 94–98.